Key Points:
- Electrostatic solitary waves (ESW) across the bow shock are Debye-scale structures with electric field oriented oblique to magnetic field
- ESW have negative electrostatic potential (they are not electron phase space holes) with amplitude of a few tenths of electron temperature
- ESW are capable of efficient pitch angle scattering, Fermi reflection, and isotropization of thermal electrons

Solitary Waves Across Supercritical Quasi-Perpendicular Shocks

I. Y. Vasko[1] [iD], F. S. Mozer[1] [iD], V. V. Krasnoselskikh[1,2] [iD], A. V. Artemyev[3,4] [iD], O. V. Agapitov[1] [iD], S. D. Bale[1,5], L. Avanov[6] [iD], R. Ergun[7] [iD], B. Giles[6] [iD], P.-A. Lindqvist[8] [iD], C. T. Russell[3] [iD], R. Strangeway[3] [iD], and R. Torbert[9] [iD]

[1]Space Sciences Laboratory, University of California, Berkeley, California, USA, [2]LPC2E, University of Orleans, France, [3]Institute of Geophysics and Planetary Sciences, University of California, Los Angeles, CA, USA, [4]Space Research Institute of Russian Academy of Sciences, Moscow, Russia, [5]Physics Department, University of California, Berkeley, CA, USA, [6]NASA, Goddard Space Flight Center, Greenbelt, MD, USA, [7]University of Colorado Boulder, Boulder, CO, USA, [8]Royal Institute of Technology, Stockholm, Sweden, [9]University of New Hampshire, Durham, NH, USA

Abstract We consider intense electrostatic solitary waves (ESW) observed in a supercritical quasi-perpendicular Earth's bow shock crossing by the Magnetospheric Multiscale Mission. The ESW have spatial scales of a few tens of meters (a few Debye lengths) and propagate oblique to a local quasi-static magnetic field with velocities from a few tens to a few hundred kilometers per second in the spacecraft frame. Because the ESW spatial scales are comparable to the separation between voltage-sensitive probes, correction factors are used to compute the ESW electric fields. The ESW have electric fields with amplitudes exceeding 600 mV/m (oriented oblique to the local magnetic field) and negative electrostatic potentials with amplitudes of a few tenths of the electron temperature. The negative electrostatic potentials indicate that the ESW are not electron phase space holes, while interpretation in terms of ions phase space holes is also questionable. Whatever is their nature, we show that due to the oblique electric field orientation the ESW are capable of efficient pitch-angle scattering and isotropization of thermal electrons. Due to the negative electrostatic potentials the ESW Fermi reflects a significant fraction of the thermal electrons streaming from upstream (downstream) back to upstream (downstream) region, thereby affecting the shock dynamics. The role of the ESW in electron heating is discussed.

Plain Language Summary Processes governing electron thermalization across shock waves are not entirely understood. The high resolution particle and 3-D electric field measurements provided by the Magnetospheric Multiscale Mission make it possible to study the Earth's bow shock that is an excellent laboratory for addressing the electron thermalization across supercritical shock waves. Previous observations showed that electron heating across the bow shock is generally governed by macroscopic cross-shock electrostatic field. On the other hand, the role of the turbulence observed across the bow shock in the electron thermalization has remained unclear. In this letter we consider a particular bow shock crossing by the Magnetospheric Multiscale Mission and focus on the role of the high amplitude electrostatic solitary waves in the electron thermalization process. We accurately estimate the electrostatic solitary wave parameters and show that due to electric fields oriented oblique to a local DC magnetic field and negative electrostatic potentials with amplitudes of a few tenths of the electron temperature, these Debye-scale structures are capable of efficient pitch angle scattering, Fermi reflection, and isotropization of thermal electrons.

1. Introduction

Electron thermalization across supercritical quasi-perpendicular shocks remains one of the unresolved problems in space plasma physics (e.g., review by Krasnoselskikh et al., 2013). Early observations of the Earth's bow shock by the ISEE mission suggested that the quasi-static cross-shock electrostatic field (rather than waves) provides the dominant contribution to electron heating (e.g., review by Scudder, 1995). Under the assumption of magnetized electron motion the cross-shock field generally results in anisotropic heating and opens up inaccessible voids in the electron phase space (e.g., Scudder, 1995). On the contrary, analysis of a particular Earth bow shock crossing by Cluster showed that the electron heating is rather isotropic and operates

predominantly within the ramp (Schwartz et al., 2011). This indicates that some mechanism of electron isotropization (pitch-angle scattering) should operate within supercritical shocks (but see also discussion by Schwartz, 2014).

Pitch-angle scattering can result from fine-scale structure of the cross-shock electrostatic field (Balikhin et al., 1998) that was observed in one of the bow shock crossings by Cluster (Walker et al., 2004). Another mechanism of the pitch-angle scattering involves electrostatic and electromagnetic waves that are observed in supercritical shocks: ion-acoustic waves (e.g., Balikhin et al., 2005; Wilson et al., 2007), electron cyclotron waves (Breneman et al., 2013), electrostatic solitary waves (ESW; Bale et al., 1998; Hobara et al., 2008), and whistler waves (e.g., Hull et al., 2012). Although electron scattering by the electrostatic waves is regularly mentioned in the literature (e.g., Mozer & Sundkvist, 2013), their effects have not been addressed in detail. The recently available 3-D electric fields measured by the Magnetospheric Multiscale Mission (MMS) make it possible to accurately estimate the properties of the electrostatic waves and address their effects.

In this letter we consider a particular bow shock crossing by MMS and focus on the largest amplitude ESW. We accurately estimate the ESW parameters and show that the ESW are not electron phase space holes (in contrast to the hypothesis of Bale et al., 1998), because they have negative electrostatic potentials. We show that due to oblique electric field orientation to a local quasi-static magnetic field and negative potentials, these Debye-scale structures are capable of efficient pitch-angle scattering, Fermi reflection, and isotropization of thermal electrons.

2. Observations

We consider the bow shock crossing on 30 November 2015 around 8:43:38 UT. We use the DC-coupled magnetic field (128 samples per second) provided by Digital and Analogue Fluxgate Magnetometers (Russell et al., 2016), AC-coupled electric fields (8,192 samples per second) provided by Axial Double Probe (Ergun et al., 2016) and Spin-Plane Double Probe (Lindqvist et al., 2016), electron temperatures and density (30-ms time resolution) provided by Fast Plasma Investigation instrument (Pollock et al., 2016). The electric field is measured by four voltage-sensitive spherical probes on 60-m booms in the spacecraft spin plane and two probes on 15-m axial booms along the spin axis. The voltages V_i (with respect to the spacecraft) of the opposing probes are used to compute the electric field in the spin plane $E_{12} = 1.8 \cdot (V_1 - V_2)/2\, l_{12}$, $E_{34} = 1.8 \cdot (V_3 - V_4)/2\, l_{34}$ and along the axial boom $E_{56} = 2.2 \cdot (V_5 - V_6)/2\, l_{56}$, where $l_{12} = l_{34} = 60$ m, $l_{56} = 15$ m, while 1.8 and 2.2 are the boom shortening factors for about 1-kHz AC-coupled signals.

Figure 1 presents the quasi-static magnetic field measured aboard MMS#1 that indicates the ramp of the supercritical shock. The upstream magnetic field of 10 nT, ion flow velocity of 460 km/s, and plasma density and temperature of 14 cm^{-3} and 70 eV (not shown here) provide the fast Alfven Mach number of about four. The shock is quasi-perpendicular with angle between the shock normal vector and the upstream magnetic field of about 86° as found using the method suggested by Vinas and Scudder (1986). Panel (b) shows that electrons are heated across the ramp from 20 to 70 eV and the heating is not entirely isotropic. Panels (c) – (f) present the electric field magnitude measured at four spacecraft and indicate that the electric field reaches amplitudes up to 450 mV/m (in fact, even higher as shown below). The waveform analysis shows that the most intense electric fields correspond to ESW.

Figure 2 presents the largest amplitude ESW observed at each MMS spacecraft. The upper panels show that the ESW electric fields parallel and perpendicular to a local magnetic field have similar bipolar profiles. For each ESW, we use the minimum variance analysis (Sonnerup & Scheible, 1998) to determine the coordinate system with vectors **L**, **M**, and **N** along directions of maximum, intermediate, and minimum electric field variation. The bottom panels show that E_L is the dominant electric field component. The angle θ between vector **L** and the local magnetic field is a few tens of degrees as indicated in the upper panels. The profile of E_L is fitted to a model bipolar profile

$$E_m(t) = E_0\,(t - t_0)/\tau \exp\left[\left(\tau^2 - (t - t_0)^2\right)/2\,\tau^2\right] \tag{1}$$

with the best fit duration τ and amplitude E_0 indicated in the bottom panels.

Because $E_{M,N} \ll E_L$, the ESW can be suggested to be approximately 1-D planar structures shown schematically in Figure 3 and modeled with the following spatial distribution of the electrostatic potential

$$\Phi = \Phi_0 \exp\left[-(z\cos\theta + x\sin\theta - v_s\, t)^2/2\, l^2\right], \tag{2}$$
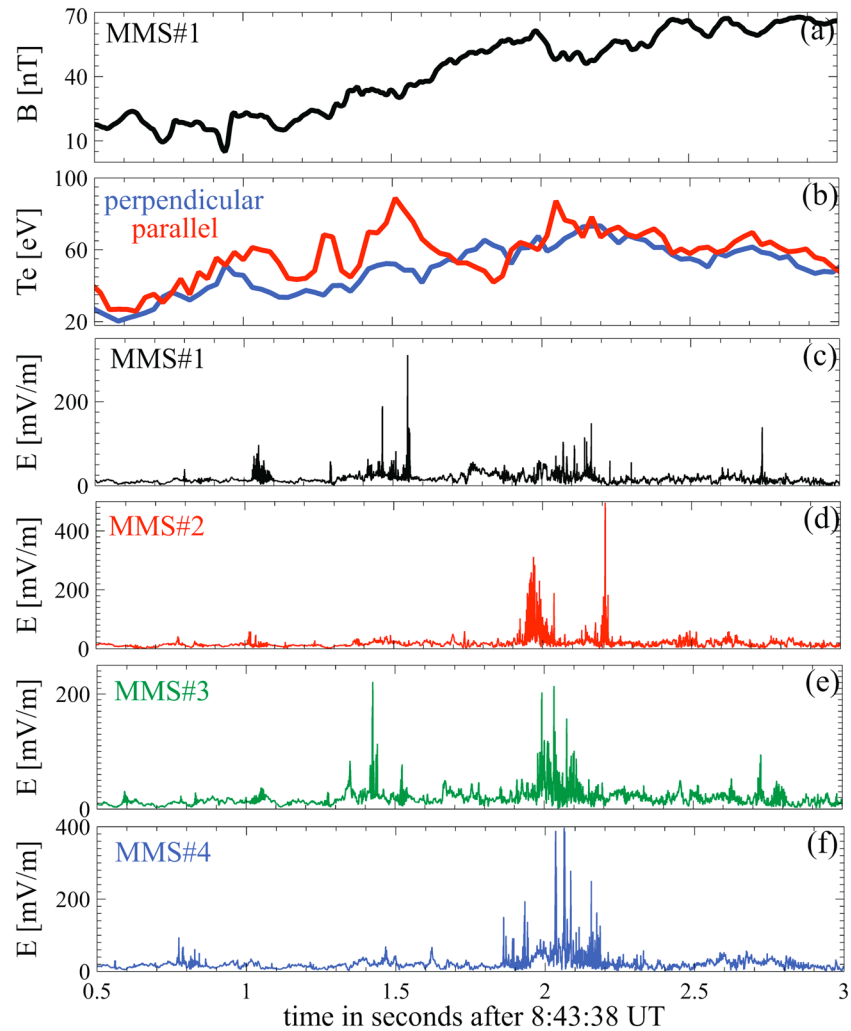
Figure 1. The bow shock crossing by MMS on 30 November 2015: (a) the magnetic field magnitude and (b) electron parallel and perpendicular temperatures measured aboard MMS#1; (c–f) magnitude of the electric fields measured at four MMS spacecraft. MMS = Magnetospheric Multiscale Mission.

where Φ_0 is the amplitude of the electrostatic potential, l is the spatial scale, v_s is the ESW velocity (e.g., in the spacecraft frame) along vector **L**, the z axis is along the local magnetic field, while vector **L** lies in the (x, z) plane (Figure 3). The probe-to-probe interferometry (analysis of time delays of the ESW occurrence at the opposing probes, see review by Mozer, 2016) makes it possible to establish whether ESW has a convergent (shown in Figure 3) or divergent electric field configuration, estimate the ESW parameters, and test applicability of the 1-D planar structure assumption.

Figure 4 presents the interferometry analysis of ESW#2, that is, the ESW observed at MMS#2. The ESW has a convergent electric field configuration, because the ESW hits probe 4 before probe 3 and E_{34} is first positive and then negative. We arrive at the same conclusion by considering the other electric fields and time delays between the other opposing probes. The time delays Δt_{ij} indicated in panels (a)–(c) are determined by cross-correlating voltages of the opposing probes. The unit vector $\mathbf{k} = (k_{12}, k_{34}, k_{56})$ along the propagation direction and the ESW velocity in the spacecraft frame are computed as $k_{ij} = v_s \Delta t_{ij}/l_{ij}$ and $v_s^{-2} = \Delta t_{12}^2/l_{12}^2 + \Delta t_{34}^2/l_{34}^2 + \Delta t_{56}^2/l_{56}^2$. We have found that $\mathbf{k} = (-0.09, 0.74, 0.66)$ and $v_s \sim 80$ km/s. For a strictly planar 1-D structure $\mathbf{k}$ and $\mathbf{L}$ have to coincide, while in our case $\mathbf{k}$ and $\mathbf{L}$ are about 30° apart. The disagreement turns out to arise, because the ESW spatial scale is comparable to the boom lengths.

The electric fields E_{ij} are fitted to the model bipolar profile (1) with the best fit parameters indicated in panels (d)–(f). We have $\tau \sim 0.45$ ms for E_{34} and $\tau \sim 0.3$ ms for E_{12} and E_{56}, so that the ESW spatial scale
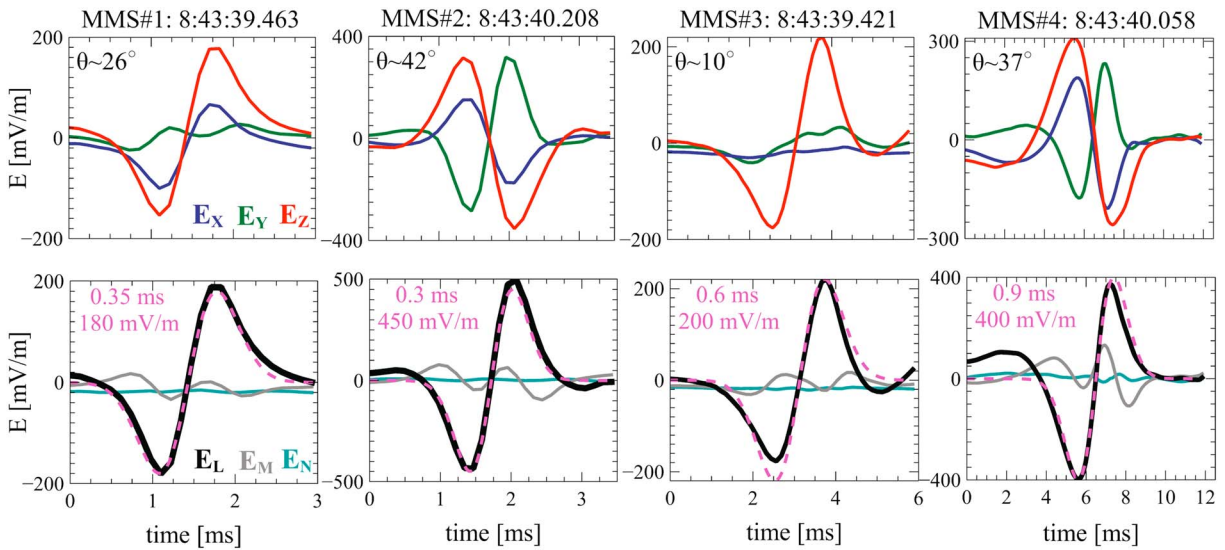
Figure 2. The largest amplitude ESW observed at each MMS spacecraft. The upper panels present the electric field components E_z and E_x, E_y that are parallel and perpendicular to a local quasi-static magnetic field, respectively. The bottom panels present the ESW electric fields in the coordinate system with vectors **L**, **M**, and **N** determined via the minimum variance analysis. The angle θ between vector **L** and the local magnetic field is indicated in the upper panels (see also Figure 3). The electric field E_L is fitted to the model bipolar electric field profile (dashed purple) with the best fit parameters τ and E_0 indicated in the bottom panels. ESW = electrostatic solitary waves.

$l = v_s\tau \sim 24\text{–}36$ m is comparable to the boom lengths. Therefore, $E_{ij} \propto (V_i - V_j)/l_{ij}$ underestimates the ESW electric field and widens the ESW electric field signal by factors that depend on $r_{ij} = l/l_{ij}|k_{ij}|$ (see the supporting information). For ESW#2 we have r_{12}, $r_{56} \gg 1$, so that E_{12} and E_{56} reproduce the original ESW electric fields and provide accurate estimate of the ESW spatial scale, $l \sim 24$ m. On the contrary, E_{34} underestimates the electric field amplitude by a factor of 2.3 and widens the ESW electric field signal by a factor of 1.5, because $r_{34} \sim 0.5$. Panel (e) presents the electric field corrected by multiplying E_{34} by factor 2.3 and by compressing the time by factor 1.5.
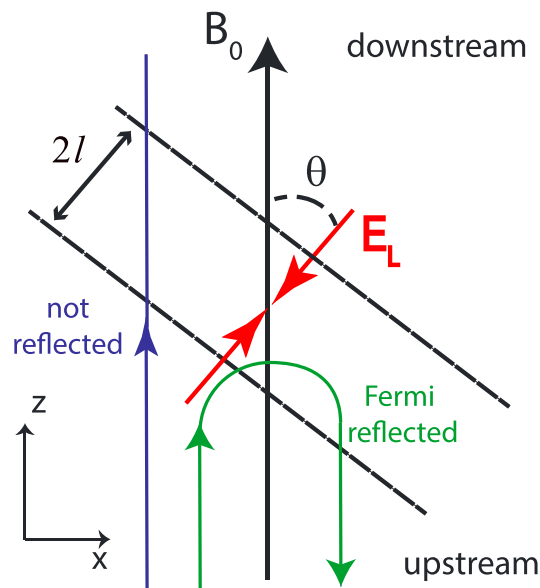

Figure 3. The schematics of approximately 1-D planar electrostatic solitary waves with a convergent electric field configuration: E_L is the dominant bipolar electric field, $2\,l$ is the typical spatial width, and θ is the electric field inclination angle to the local DC magnetic field **B**$_0$. Thermal electrons streaming from the upstream (downstream) region can be either Fermi reflected back to the upstream (downstream) region or pass through.
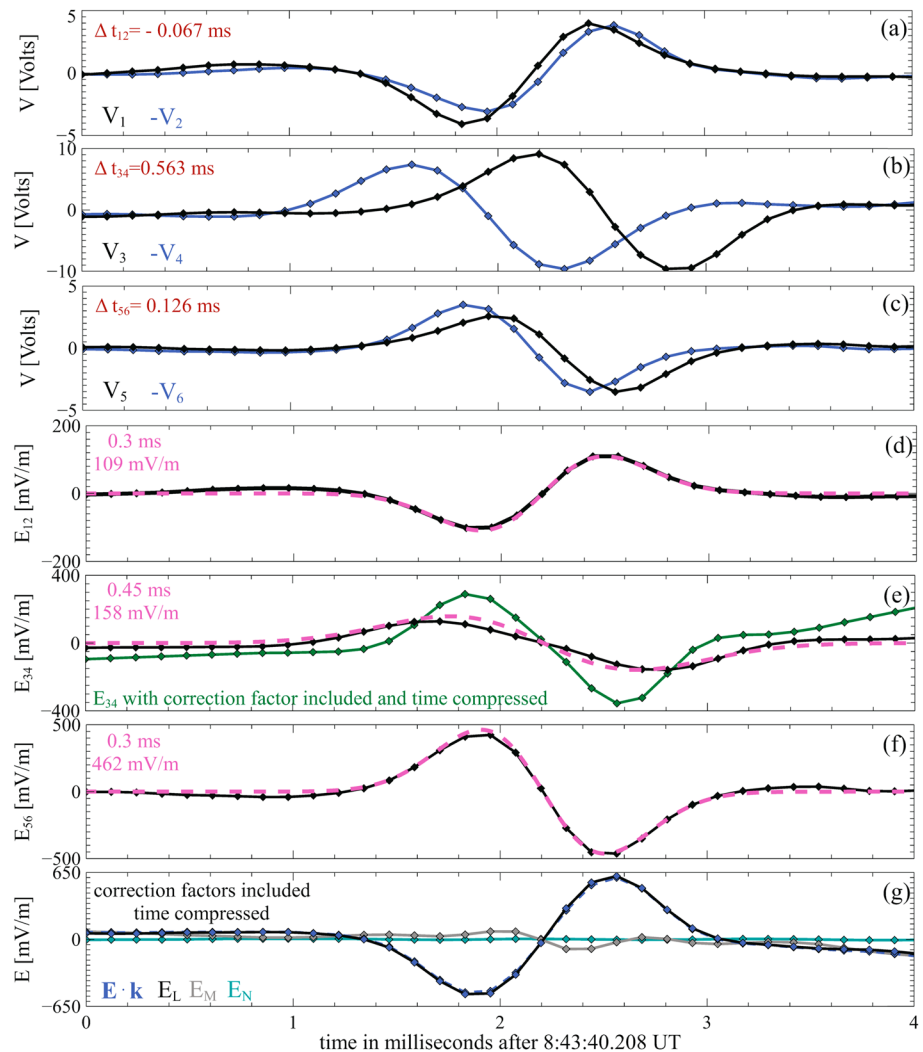
Figure 4. The interferometry analysis of the ESW observed aboard MMS#2: (a–c) voltages V_1 and $-V_2$, V_3 and $-V_4$, V_5, and $-V_6$; the time delays Δt_{ij} between the opposing probes are indicated; (d–f) electric fields in the spin plane E_{12}, E_{34}, and along the axial boom E_{56}; the electric fields are fitted to the model bipolar profile (dashed purple) with the best fit parameters indicated in the panels; panel (e) also shows E_{34} multiplied by the correction factor 2.3 and plotted versus time compressed by factor 1.5 (see section 2 for details); (g) the corrected electric field in the coordinate system determined by the MVA. ESW = electrostatic solitary waves; MMS = Magnetospheric Multiscale Mission; MVA = minimum variance analysis.

Figure 4g presents the corrected electric field in the coordinate system determined by the minimum variance analysis. First, the correction of the electric fields decreases the angle between **k** and **L** to 9° implying that ESW#2 can be considered as approximately 1-D planar structure. Second, the angle θ between **L** and a local magnetic field turns out to be about 20° rather than 40°. This implies that ESW#2 actually has oblique electric field and propagates oblique to the local magnetic field. Third, the ESW electric field amplitude is 615 mV/m rather than 450 mV/m. The convergent electric field configuration implies that ESW#2 has a negative electrostatic potential with amplitude $\Phi_0 = -max(E_L) \; l \; \exp(1/2) \sim -24$ V that is a significant fraction of the electron temperature, $T_e \sim 70$ eV. Because the plasma density is about 40 cm^{-3}, the ESW spatial scale is a few Debye lengths, $l \sim 1.7 \; \lambda_D$.

Table 1 summarizes results of analysis of the other ESW presented in Figure 2. Vectors **k** and **L** are at least 60° apart, and the correction of the electric fields significantly reduces this angle only for ESW#4. Any reasonable variation of the boom shortening factors does not produce significantly better agreement between **k** and **L** for ESW#1 and #3. This implies that the ESW cannot be generally considered as 1-D planar structures. Nevertheless, we present estimates of the ESW parameters computed analogously to ESW#2. The ESW have

Table 1
Parameters of the Largest Amplitude ESW Observed at Each MMS Spacecraft

ESW	$\cos^{-1}$ (**kL**)	v_s	l	$max(|E_L|)$	Φ_0	l/λ_D	$|\Phi_0|/T_e$
		km/s	m	mV/m	V		
#1	62°/ 50°	150	50	210	−17	3.2	0.3
#2	30°/ 9°	80	24	615	−24	1.7	0.34
#3	75°/ 60°	80	44	230	−17	3.2	0.24
#4	62°/ 30°	30	23	540	−20	1.7	0.28

Note. $\cos^{-1}$ (**kL**) is the angle between **k** and **L** computed before and after inclusion of the correction factors; v_s is the ESW velocity in the spacecraft frame, l is the spatial scale, $max(|E_L|)$ is the electric field amplitude, Φ_0 is the amplitude of the electrostatic potential; and λ_D and T_e are local Debye length and electron temperature. ESW = electrostatic solitary waves; MMS = Magnetospheric Multiscale Mission.

spatial scales of a few tens of meters and electric field amplitudes of a few hundred mV/m. They have the convergent electric field configuration and amplitudes of negative electrostatic potentials of a few tenths of the electron temperature.

About 20 ESW observed at four MMS spacecraft in the shock are presented in the supporting information. Similarly to the largest amplitude ESW, they have the convergent electric field configuration. The analysis of the ESW electric fields (with no corrections) has shown that $\theta \sim 35°$, $E_0 \sim 100$ mV/m, and $\tau \sim 0.3-0.5$ ms are rather typical parameters. Assuming the ESW velocity of about 100 km/s, we find the typical spatial scale of a few tens of meters that is comparable to the boom lengths. Therefore, the correction factors should be used to compute the actual ESW electric field amplitudes and inclination angles.

3. Electron Scattering

We run a test-particle simulation to demonstrate the scattering by a single ESW in a uniform local magnetic field. We adopt parameters of ESW#2 ($\Phi_0 = -24$ V, $l = 24$ m, and $\theta = 20°$) and the local magnetic field of about 50 nT (Figure 1). We also run simulations for similar ESW, but with $\theta = 40°$. The scattering is considered in the reference frame propagating with velocity $v_s / \cos\theta$ along the magnetic field (with respect to the spacecraft), where according to equation (2), the ESW electrostatic potential is stationary. Thermal electrons are launched from the upstream to downstream region and in the opposite direction that corresponds to pitch angles $\alpha \in [0°, 90°)$ and $(90°, 180°]$ (Figure 3). In the selected reference frame, the electron energy is conserved and only pitch-angle scattering occurs.

Figure 5 presents the pitch-angle scattering of 20- to 50-eV electrons ($3 \cdot 10^5$ electrons are traced for each energy). Because the ESW electrostatic potential is negative, there are Fermi reflected electrons and electrons passing through the ESW (as illustrated in Figure 3). We can see that 20-eV electrons (in fact, all electrons below about 24 eV) are Fermi reflected. In the case of the strictly parallel electric field orientation ($\theta = 0°$) Fermi reflection would scatter electrons with pitch angle α to pitch angle $180°-\alpha$ without any change in the magnetic moment. The oblique orientation provides the perpendicular electric field component that makes possible the nontrivial pitch-angle scattering (i.e., the magnetic moment changes). The pitch-angle scattering of electrons below about 40 eV can be quite pronounced, for example, 45° electron can become 180°, implying that the oblique electric field orientation may provide nontrivial scattering by 45°. A significant fraction of ≲40-eV electrons is Fermi reflected, but there are also electrons passing through the ESW. At higher energies the fraction of Fermi reflected electrons (indicated in the upper and middle panels of Figure 5) decreases and the scattering becomes less efficient.

To demonstrate effects of the scattering on evolution of the electron pitch-angle distribution (PAD), we assume electrons streaming from upstream to downstream and in the opposite direction to have field-aligned PAD, for example, $PAD(\alpha) = 1 + 0.5\cos^2\alpha$. Using the Liouville theorem and the test-particle results, we compute PAD after the scattering by the ESW with $\theta = 20°$ and 40°. Figure 5 shows that PAD of 30 eV (and lower energy) electrons becomes rather isotropic, except at $\alpha \sim 90°$, because of inefficient scattering at these pitch angles. The anisotropy of 40- and 50-eV electrons is also significantly reduced. At higher energies the anisotropy reduces, but the effect is less pronounced than below 50 eV.
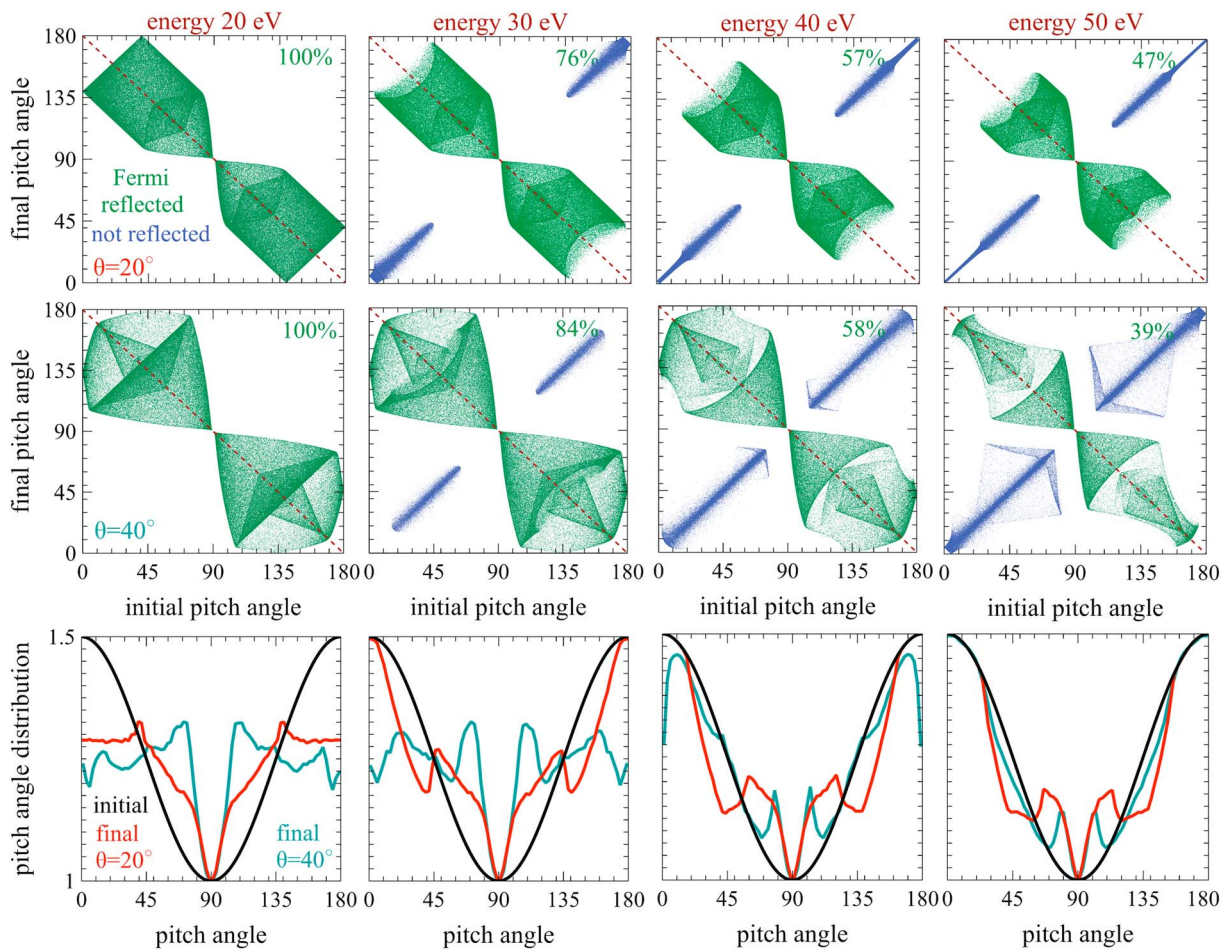
Figure 5. The results of the test-particle simulation of the electron scattering by ESW#2 (upper panels) and by similar ESW with inclination angle $\theta = 40°$ (middle panels). The upper and middle panels present the pitch angle before and after the scattering for 20- to 50-eV electrons. The fraction of Fermi reflected electrons is indicated in the panels. The dashed line corresponds to the scattering that would be driven by ESW with only parallel electric field ($\theta = 0°$): Fermi reflected electron with initial pitch angle α would have final pitch angle $180° - \alpha$. The bottom panels present how the scattering by the ESW modifies the pitch-angle distribution of initially field-aligned electrons (black curve). ESW = electrostatic solitary waves.

In the ESW reference frame the scattering occurs only in pitch angle, but in the spacecraft frame electron energy is certainly not conserved. In this frame $(v_z - v_s / \cos \theta)^2 + v_\perp^2 = \text{const}$, so that the energy and pitch-angle variations are related to each other

$$\Delta w = 2 (w w_s)^{1/2} \Delta(\cos \alpha),$$

where $w_s = m_e (v_s / \cos \theta)^2 / 2$, w is the energy in the ESW frame, and $\Delta(\cos \alpha)$ is the variation of $\cos \alpha$ due to the scattering. For realistic parameters $v_s / \cos \theta \sim 200$ km/s, so that $w_s \sim 0.1$ eV. The maximum energy gain or loss per single scattering $4 (w \cdot 0.1 \text{ eV})^{1/2}$ is realized for Fermi-reflected electrons. Electrons with energies 10–100 eV can gain or lose about 5–10 eV due to a single interaction that is generally nonnegligible. The net efficiency of the electron heating depends on the number of scattering events electrons experience across the shock and on the electron velocity distribution function that determines number of particles gaining and losing energy. The previous observations suggest that this mechanism is less efficient than the heating by the quasi-static cross-shock electrostatic field (e.g., Scudder, 1995).

4. Discussion and Conclusion

In this letter we have used 3-D electric fields measured by the MMS for analysis of the largest amplitude ESW observed in a particular Earth's bow shock crossing. The ESW have spatial scales comparable to the boom lengths that is why the accurate analysis (including the corrections factors) has been carried out to estimate the ESW parameters and test applicability of the 1-D planar structure assumption. The ESW considered

in detail is approximately 1-D planar structure with electric field amplitude exceeding 600 mV/m that is comparable to the largest electric fields ever observed across the Earth's bow shock (Bale & Mozer, 2007). The ESW is the Debye-scale structure propagating oblique to a local quasi-static magnetic field (for 1-D structures only velocity along **k** is measurable) and having a negative electrostatic potential with amplitude of a few tenths of the electron temperature. We have also found that some of the considered ESW are likely not 1-D planar structures.

The presented ESW are identical to $\sim$ 100 mV/m ESW reported previously and interpreted in terms of electron phase space holes (the Bernstein-Green-Kruskal mode with trapped electrons, see Schamel, 1982) based on their Debye-scale spatial widths (Bale et al., 1998). The ESW presented in this letter cannot be electron phase space holes, because they have negative electrostatic potentials. Along with previous observations of much less intense ESW with negative potential (Hobara et al., 2008), this letter provides motivation for a careful statistical reanalysis of the ESW observed across the Earth's bow shock.

The ESW velocities comparable to the ion thermal velocity suggest interpretation in terms of ion phase space holes, which formation across shocks was demonstrated in 1-D particle in cell simulations (e.g., Shimada & Hoshino, 2004). However, due to the oblique electric field orientation to a local magnetic field ion phase space holes could not remain coherent, because the ESW spatial scales are many times smaller than the typical ion thermal gyroradius (that is about a few tens of kilometers). The interpretation in terms of ion phase space holes is hence questionable. Alternatively, the ESW can be ion-acoustic solitons (Chanteur & Raadu, 1987), but this hypothesis should be tested in the future. The mechanisms capable of generating the observed large-amplitude ESW propagating oblique to a local magnetic field remain unclear.

We have shown that due to the oblique electric field, the ESW violate magnetized motion of thermal electrons. Even a single scattering by a large-amplitude ESW can provide efficient isotropization of thermal electrons below about 40 eV. At higher energies the anisotropy reduction is less pronounced, but encounter with several such ESW can result in significant effect at these energies. We have also demonstrated that due to the negative electrostatic potential and amplitude of a few tenths of the electron temperature, the ESW Fermi reflect a significant fraction of the thermal electrons streaming from upstream (downstream) back to upstream (downstream) region, thereby affecting the shock dynamics. Thus, the scattering by the ESW can reduce anisotropy of thermal electrons and infill voids in the electron phase space that are opened up by electron transport in the quasi-static magnetic and cross-shock electrostatic field (e.g., Scudder, 1995).

Finally, we summarize our conclusions:

1. The ESW observed across the selected shock are Debye-scale structures propagating oblique to a local quasi-static magnetic field, having electric fields oriented oblique to the local magnetic field and negative electrostatic potentials. Therefore, the ESW are not electron phase space holes, while interpretation in terms of ion phase space holes is also questionable.
2. The ESW drive pitch-angle scattering of thermal electrons (violate their magnetized motion) and can provide efficient isotropization of electrons even due to a single scattering event.
3. Due to negative electrostatic potentials, the ESW can Fermi reflect a significant fraction of the thermal electrons from upstream (downstream) back to upstream (downstream) region, thereby affecting the shock dynamics.

References

Bale, S. D., Kellogg, P. J., Larsen, D. E., Lin, R. P., Goetz, K., & Lepping, R. P. (1998). Bipolar electrostatic structures in the shock transition region: Evidence of electron phase space holes. *Geophysical Research Letters*, *25*, 2929–2932. https://doi.org/10.1029/98GL02111

Bale, S. D., & Mozer, F. S. (2007). Measurement of large parallel and perpendicular electric fields on electron spatial scales in the terrestrial bow shock. *Physical Review Letters*, *98*(20), 205001. https://doi.org/10.1103/PhysRevLett.98. 205001

Balikhin, M., Krasnosel'skikh, V. V., Woolliscroft, L. J. C., & Gedalin, M. (1998). A study of the dispersion of the electron distribution in the presence of E and B gradients: Application to electron heating at quasi-perpendicular shocks. *Journal of Geophysical Research*, *103*, 2029–2040. https://doi.org/10.1029/97JA02463

Balikhin, M., Walker, S., Treumann, R., Alleyne, H., Krasnoselskikh, V., Gedalin, M., et al. (2005). Ion sound wave packets at the quasiperpendicular shock front. *Geophysical Research Letters*, *32*, L24106. https://doi.org/10.1029/2005GL024660

Breneman, A. W., Cattell, C. A., Kersten, K., Paradise, A., Schreiner, S., Kellogg, P. J., et al. (2013). STEREO and Wind observations of intense cyclotron harmonic waves at the Earth's bow shock and inside the magnetosheath. *Journal of Geophysical Research: Space Physics*, *118*, 7654–7664. https://doi.org/10.1002/2013JA019372

Chanteur, G., & Raadu, M. (1987). Formation of shocklike modified Korteweg-de Vries solitons — Application to double layers. *Physics of Fluids*, *30*, 2708–2719. https://doi.org/10.1063/1.866036

Ergun, R. E., Tucker, S., Westfall, J., Goodrich, K. A., Malaspina, D. M., Summers, D., et al. (2016). The axial double probe and fields signal processing for the MMS Mission. *Space Science Reviews*, *199*, 167–188. https://doi.org/10.1007/s11214-014-0115-x

Hobara, Y., Walker, S. N., Balikhin, M., Pokhotelov, O. A., Gedalin, M., Krasnoselskikh, V., et al. (2008). Cluster observations of electrostatic solitary waves near the Earth's bow shock. *Journal of Geophysical Research*, *113*, A05211. https://doi.org/10.1029/2007JA012789

Hull, A. J., Muschietti, L., Oka, M., Larson, D. E., Mozer, F. S., Chaston, C. C., et al. (2012). Multiscale whistler waves within Earth's perpendicular bow shock. *Journal of Geophysical Research*, *117*, A12104. https://doi.org/10.1029/2012JA017870

Krasnoselskikh, V., Balikhin, M., Walker, S. N., Schwartz, S., Sundkvist, D., Lobzin, V., et al. (2013). The synamic quasiperpendicular shock: Cluster discoveries. *Space Science Reviews*, *178*, 535–598. https://doi.org/10.1007/s11214-013-9972-y

Lindqvist, P.-A., Olsson, G., Torbert, R. B., King, B., Granoff, M., Rau, D., et al. (2016). The Spin-Plane Double Probe Electric Field Instrument for MMS. *Space Science Reviews*, *199*, 137–165. https://doi.org/10.1007/s11214-014-0116-9

Mozer, F. S. (2016). DC and low-frequency double probe electric field measurements in space. *Journal of Geophysical Research: Space Physics*, *121*, 10,942–10,953. https://doi.org/10.1002/2016JA022952

Mozer, F. S., & Sundkvist, D. (2013). Electron demagnetization and heating in quasi-perpendicular shocks. *Journal of Geophysical Research: Space Physics*, *118*, 5415–5420. https://doi.org/10.1002/jgra.50534

Pollock, C., Moore, T., Jacques, A., Burch, J., Gliese, U., Saito, Y., et al. (2016). Fast Plasma Investigation for Magnetospheric Multiscale. *Space Science Reviews*, *199*, 331–406. https://doi.org/10.1007/s11214-016-0245-4

Russell, C. T., Anderson, B. J., Baumjohann, W., Bromund, K. R., Dearborn, D., Fischer, D., et al. (2016). The Magnetospheric Multiscale Magnetometers. *Space Science Reviews*, *199*, 189–256. https://doi.org/10.1007/s11214-014-0057-3

Schamel, H. (1982). Kinetic theory of phase space vortices and double layers. *Physica Scripta Volume T*, *2*, 228–237. https://doi.org/10.1088/0031-8949/1982/T2A/030

Schwartz, S. J. (2014). Comment on "Electron demagnetization and heating in quasi-perpendicular shocks" by Mozer and Sundkvist. *Journal of Geophysical Research: Space Physics*, *119*, 1507–1512. https://doi.org/10.1002/2013JA019624

Schwartz, S. J., Henley, E., Mitchell, J., & Krasnoselskikh, V. (2011). Electron temperature gradient scale at collisionless shocks. *Physical Review Letters*, *107*(21), 215002. https://doi.org/10.1103/PhysRevLett.107.215002

Scudder, J. D. (1995). A review of the physics of electron heating at collisionless shocks. *Advances in Space Research*, *15*, 181–223. https://doi.org/10.1016/0273-1177(94)00101-6

Shimada, N., & Hoshino, M. (2004). Electron heating and acceleration in the shock transition region: Background plasma parameter dependence. *Physics of Plasmas*, *11*, 1840–1849. https://doi.org/10.1063/1.1652060

Sonnerup, B. U. Ö., & Scheible, M. (1998). Minimum and maximum variance analysis. *ISSI Scientific Reports Series*, *1*, 185–220.

Vinas, A. F., & Scudder, J. D. (1986). Fast and optimal solution to the 'Rankine-Hugoniot problem'. *Journal of Geophysical Research*, *91*, 39–58. https://doi.org/10.1029/JA091iA01p00039

Walker, S., Alleyne, H., Balikhin, M., André, M., & Horbury, T. (2004). Electric field scales at quasi-perpendicular shocks. *Annales Geophysicae*, *22*, 2291–2300. https://doi.org/10.5194/angeo-22-2291-2004

Wilson, L. B., Cattell, C., Kellogg, P. J., Goetz, K., Kersten, K., Hanson, L., et al. (2007). Waves in interplanetary shocks: A Wind/WAVES study. *Physical Review Letters*, *99*(4), 41101. https://doi.org/10.1103/PhysRevLett.99.041101